Title

Design Rules for Self-Assembly of 2D Nanocrystal/Metal–Organic Framework Superstructures

Journal

Angewandte Chemie, 130(40)

ISSN

0044-8249

Authors

Qiu, Fen

Edison, John R

Preisler, Zdenek

et al.

Publication Date

2018-10-01

DOI

10.1002/ange.201807776

Design Rules for Self-Assembly of Nanocrystal-Metal Organic Framework Superstructures

Fen Qiu,[1] Yan-Fang Zhang,[2] Guo Li,[1] Aizhao Pan,[1] Chih-Hao Hsu,[1] Tracy M. Mattox,[1] Peter Ercius,[3] Chengyu Song,[3] Karen Bustillo,[3] Mike Brady,[4] Sohee Jeong,[1] Steve Whitelam,[1] Jeffrey Neaton,[1] Shixuan Du,[2] Jeffrey J. Urban[1]*

1. The Molecular Foundry, Lawrence Berkeley National Laboratory, 1 Cyclotron Road, Berkeley, California 94720, USA.

2. Institute of Physics & University of Chinese Academy of Sciences, Chinese Academy of Sciences, Beijing 100190, China

3. National Center for Electron Microscopy, The Molecular Foundry, Lawrence Berkeley National Laboratory, Berkeley, California 94720, USA.

4. Advanced Light Source, Lawrence Berkeley National Laboratory, Berkeley, California 94720, USA.

Correspondence and requests for materials should be addressed to J.J.U.

(email: jjurban@lbl.gov).

Dimensionally controlled inorganic nanocrystals (NCs) and metal organic frameworks (MOF) are two powerful fields of materials science, each providing new approaches to energy storage, conversion, and catalysis[1-2]. However, despite the allure of uniting the complementary functions of these two materials into hybrid assemblies exhibiting enhanced gas storage or catalytic behavior, this has proven challenging in practice due to lack of synthetic control over essential NC-MOF interfaces. Currently, the only hybrid assemblies reported are variants on a core-shell or controlled encapsulation scheme, and no general rules of design exist that govern co-assembly or synthesis[3]. Therefore, these *ad hoc* approaches are intrinsically limited and also critically sacrifice the performance of the materials for transport and catalysis due to the encapsulated topology. Here, we demonstrate for the first time the guiding principles behind simple self-assembly of MOF nanoparticles (NPs) and oleic acid capped iron oxide (Fe_3O_4) NCs into a uniform two-dimensional bi-layered superstructure, advancing a new concept for design and self-assembly of MOFs and NCs into high surface area assemblies, mimicking the structure of supported catalyst architectures. This self-assembly process can be controlled by the energy of ligand-ligand interactions between surface ligands on Fe_3O_4 NCs and $Zr_6O_4(OH)_4(fumarate)_6$ MOF NPs. Scanning transmission electron microscopy (STEM)/energy-dispersive X-ray spectroscopy and TEM tomography confirm the hierarchical co-assembly of Fe_3O_4 NCs with MOF NPs as ligand energies are manipulated to promote facile diffusion of the smaller NCs. First principles calculations and Monte Carlo simulations were used to understand the different regimes of self-assembly, further confirming our hypothesis regarding the dominant role that ligand interactions play in self-assembly. This study opens a new avenue for co-assembly of MOF NPs with inorganic NCs

as a new type of functional material or specially designed tandem catalyst, and provides the first insight into the kinetic processes occurring in MOF-based NP self-assembly.

The engineering of nanoparticles (NPs) into well-defined superstructures has provided new insight into the processes of self-assembly and has also enabled technological applications in electronics[4], optics[5], catalysis[2, 6] and biomedicine[7]. Spatially organized combinations of various types of semiconductors, metals and magnetic nanoparticles have led to the emergence of novel collective properties of the superstructured assemblies through a close interaction between different components in ordered geometries.[8-12] However, merely mixing different types of NPs together seldom leads to self-assembly, and instead often results in uncontrolled phase segregation. It has been revealed that the self-assembly of colloidal inorganic NCs into highly ordered superlattices through spontaneous formation processes[13-14] is dictated by the entropic and energetic interactions between NCs[15]. When a binary mixture of NPs is closely packed by volume, the self-assembly process can be accurately described by a hard-sphere model, which indicates that the entropy is the predominant driving force. Such a model requires excellent size and shape uniformity of the NPs for ordered geometries[16]. Due to strict requirements on the size and shape of NPs for self-assembly, inclusion of metal organic frameworks (MOFs) into assembly phenomena is challenging, given that the size and morphology of MOFs are difficult to control. However, the energetic interaction between the organic ligands on the NP surfaces also has been shown to act as a key driving force that controls self-assembly.[17-18] Besides utilizing the conformational entropy as the driving force for self-assembly, ligand interaction can also be used to optimize self-assembly. This concept has been demonstrated by the field of NC-DNA assemblies, where ligand interaction is the main driving force and the NPs become decorations on the DNA scaffold.

At present, a few groups have identified ways to specifically attach MOFs to substrates in order to harness their potential utilities. MOF are comprised of a high surface area porous organic skeleton with programmable pendant chemical groups as linkers that connect open metal sites. Their structure suggests that MOF containing materials could be specifically designed for catalysis applications.[19-22] Thus, MOFs have been recognized as a promising candidate to become superstructure building blocks with desired functionalities. In addition, iron oxide (Fe_3O_4) NCs are widely used for catalysis and electrochemical energy storage, and are amongst the most common building blocks for controlled self-assembly because of their narrow size distribution achieved by large-scale colloidal synthesis.

In this study, we adapted the air-liquid interface assembly method to the co-self-assembly of MOF NPs with inorganic Fe_3O_4 NCs[23]. (Scheme 1) This method has been generally used for forming binary inorganic NC superlattices, and we adapted this method to form the Fe_3O_4-MOF superstructures in our studies. In our binary system, ∽50 nm diameter $Zr_6O_4(OH)_4(fumarate)_6$ MOF NPs are assembled with ∽12 nm diameter inorganic Fe_3O_4 NCs with the size ratio 4:1, which is the largest size difference reported between two NPs used for self-assembly.

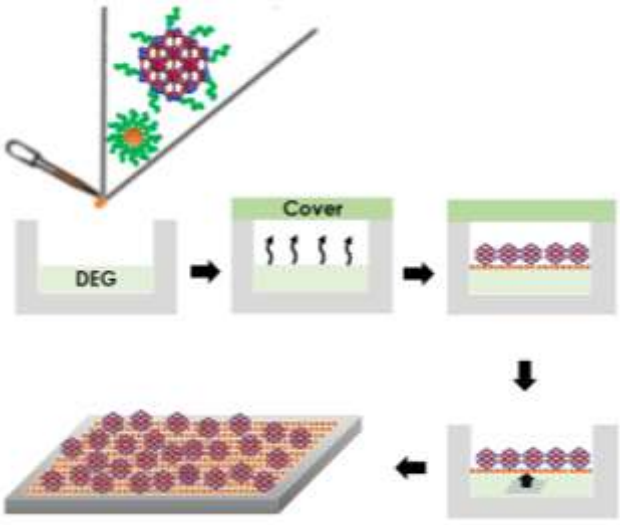

Scheme 1 Cartoon of the 2-D bi-layered superstructure film growth and transfer processes.

Figure 1a shows a representative scanning transmission electron microscopy (STEM) image of the superstructure self-assembled from oleic acid capped Fe_3O_4 (OA-Fe_3O_4) and OA-MOF NPs, clearly revealing that the two sets of NPs uniformly integrate into different layers. It also suggests that the OA-Fe_3O_4 NCs form locally ordered hexagonal superlattices while the MOF NPs maintain uniform packing into one single layer. Elemental mapping using energy-dispersive X-ray spectroscopy (EDX) confirmed each component in the system was either a MOF containing Zr or a Fe_3O_4 NC represented by the Fe element. (Figure 1b) However, the lateral structure of the co-assembly was still ambiguous, as the projection images cannot distinguish between two possible structures: i. Fe_3O_4 and MOF as separated layers; ii. Fe_3O_4 conformally covers the surface of the MOF. In order to understand how the two types of NPs co-assembled in the lateral plane, three-dimensional (3D) transmission electron microscopy tomographic images were acquired. The tilt series was fed into an iterative tomographic reconstruction algorithm to obtain a three-dimensional rendering of the superstructure, showing the bi-layered superstructure system (Figure 1c). The image of the cross-section achieved after reconstruction confirms that the MOF NPs formed a single layer on top of a mono-layered Fe_3O_4 NC superlattice (Figure 1d). A 3D 360° rendering provided a vivid animation (Supplementary Information) showing the excellent uniformity of the bilayer superstructure. In this binary system, the layer of Fe_3O_4 NP superlattice is closely connected to the MOF layer, suggesting a powerful approach for designing a supported catalyst. In order to understand the uniformity of the binary system, the average interparticle distance between OA-Fe_3O_4 NPs was measured to be 14.5 nm (Figure S1), which is consistent with the interparticle distance of the single component superlattice of OA-Fe_3O_4 NPs measured from TEM images. (Figure S2) In addition, the

measured inter-particle distance between MOF NPs in this bi-layered superstructure is 58±15 nm, suggesting a high degree of uniformity in the nanostructured bilayer. (Figure S1) In this self-assembly process, although the size of the MOF NP is not uniform, the achieved long-range hexagonal ordered OA capped Fe_3O_4 superlattice worked as a supporting template to facilitate a single layer MOF film sitting on its top surface, forming a 2D bi-layered superstructure. The monolayer of MOF on top of the Fe_3O_4 NP superlattice is more compact and uniform, compared to the single component MOF film (Figure S3) which suggests that there is an interaction between the two layers of NPs. It should be noted that there are areas where the single component MOF assembly or Fe_3O_4 assembly co-existed and mixed with the bi-layered superstructures, but the uniform MOF-Fe_3O_4 bi-layered superstructures produced in the area where the Fe_3O_4 formed superlattices below is predominantly covering the entire film. It should also be noted that the 2D bi-layered superstructure was observed when the concentration of Fe_3O_4 was larger than MOF in the mixed solution of the assembly process. This promotes the hypothesis that the Fe_3O_4 NP superlattice might assemble prior to MOF self-assembly; the diffusion kinetics of the two different types of NPs might drive the formation of the 2D bi-layered superstructure.

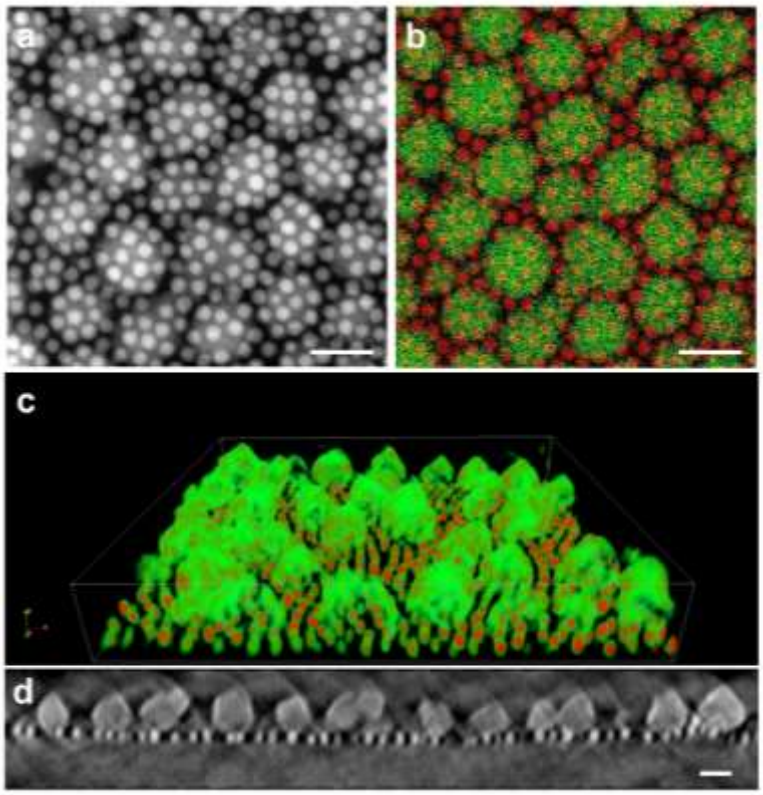

Figure 1. Electron microscopy Images of self-assembled NC-MOF bi-layered superstructure. a. STEM image of the 2-D bi-layered superstructure film (scale bar is 50 nm). **b**. STEM/EDX confirms the element of each NP (red is Fe-Kα and green is the sum of Zr-Kα and Zr-Lα, scale bar is 50 nm). **c.** 3D rendering of the 3D TEM tomography reconstruction. The false color is only as a guide to the reader, red corresponds to Fe representing Fe_3O_4 NCs, green corresponds to Zr representing MOF NPs. **d** Cross-section from the 3D tomography reconstruction showing the 2D bi-layered superstructure film (scale bar is 70 nm).

According to Fick's first law, the diffusive flux is the product of diffusion coefficient (diffusivity), and the driving force of each species. In our system, the OA-Fe_3O_4 NCs diffuse faster than MOF NPs in the precursor droplet because the diffusivity of a spherical NP is inversely proportional to the radius of sphere based on the Stokes-Einstein equation. This hypothesis does not include the energetic term, which will be considered later in the Monte Carlo simulations. When the droplet of solution is released in the air-liquid interface during self-assembly, the large numbers of OA-Fe_3O_4 NCs form a large area of compact superlattice while MOF NPs do not have space to insert into the Fe_3O_4 NC superlattice plane. Thus, the MOF NPs

sit on top of the Fe_3O_4 layer. The uniform bi-layered superstructure area can be as large as 1 μm as shown in Figure 2a. In order to study how the energetic interaction influences the self-assembly, the surface ligands of Fe_3O_4 were changed from OA to polystyrene (PS), a grafted polymer with higher molecular weight while retaining softness and strong ligand-ligand interactions, which leads to change of the energetic interaction in the diffusion rate definition based on Fick's first law. Under the same self-assembly condition for assemble PS- Fe_3O_4 NCs with MOF NPs (details in SI), we observed that PS-Fe_3O_4 NCs were separated by MOF NPs in the same plane, and the bigger MOF NPs were surrounded by smaller PS-Fe_3O_4 NCs, (Figure 2b) indicating a simultaneous diffusion of the two types of NPs to form a single layer. Resonant soft x-ray scattering (RSoXS) showed a hexagonal order corresponding to the superlattice layer of Fe_3O_4 formed in both samples, but the x-ray intensity was higher in the OA-Fe_3O_4-MOF system. (Figure S4) The higher x-ray intensity in the OA-Fe_3O_4-MOF sample indicates more hexagonal order area in the bilayer superstructures; in the PS-Fe_3O_4 and MOF system, insertion of MOF into the Fe_3O_4 superlattice plane leads to less hexagonal order. The largest Fe_3O_4 NC spacing was measured to be 13.05 nm when the surface organic ligand is OA as compared to 13.27 nm when the surface organic ligand is PS. This increased inter-particle distance in the PS-Fe_3O_4 NC superlattice after ligand exchange is significant and consistent with the FFT calculations, indicating that the PS ligand is longer than OA capping on the surface of the Fe_3O_4 NCs. The absolute value is different from the FFT measurements most likely because of the larger average area (200 μm) illuminated by RSoXS and because of the different substrates used for these two measurements.

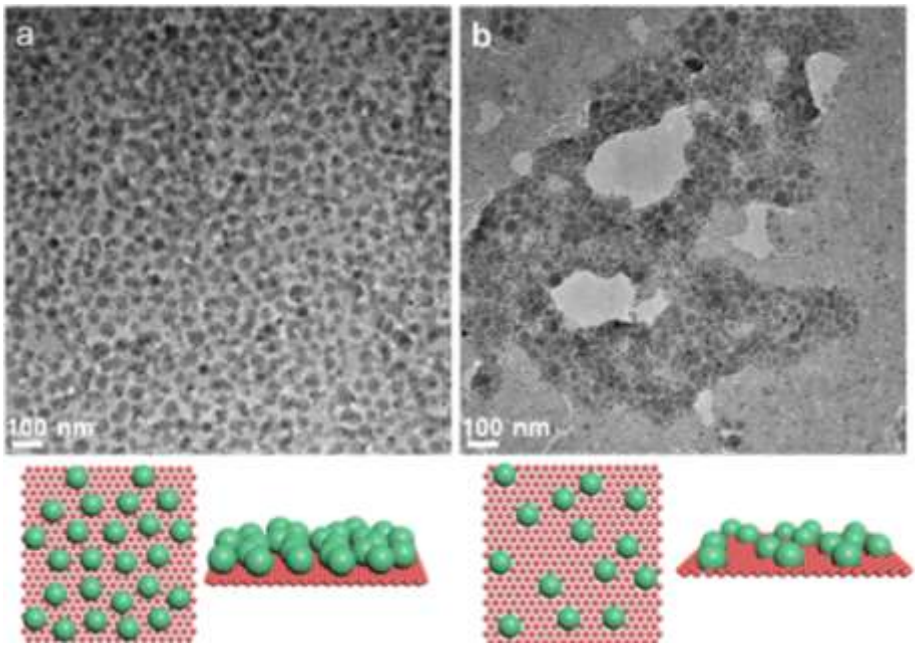

Figure 2. TEM images of films co-assembled by MOF and Fe_3O_4 NCs with different ligands a is with OA as ligands **b** is with PS as ligands. The cartoons illustrate the self-assembly of two processes due to the different surface ligands of Fe_3O_4 NCs representing TEM images above respectively: red sphere represents Fe_3O_4 NCs, green sphere represents MOF NPs.

In our systems, the two different assembly processes are only distinguished by the surface ligands of Fe_3O_4 NCs, which mainly contribute to the energetic interactions in the co-assembly process. To understand this phenomenon, we performed First Principles Calculations based on density functional theory (DFT) and found that the inter-layer interactions are dramatically different for OA and PS. The DFT results suggest that interaction energy between OA films is 9 meV/formula, much lower than the interaction energy for PS films of 314 meV/formula, indicating a much stronger interaction of PS films than that of OA films. Further, the interaction energy between MOF NPs was represented by calculating the organic linker fumaric acid as the organic linker is predominant in MOF structure due to the low metal density for framework, which lead to relatively less surface capping ligands compared to inorganic NCs, and the resulted energy is 245 meV/formula, which is close the PS film, indicating the close diffusion rate for MOF compared to PS-Fe_3O_4 NCs.

Furthermore, we evaluated the rates for a series microprocessor involved in the self-assembly based on the DFT results, and carried out kinetic Monte Carlo (MC) simulations to reveal how the final patterns of self-assembly are affected by the ligands (details can be found in the SI). In the simulations, we considered a series of atomic processes relevant to the process of self-assembly: i. diffusion of NPs on top of a NP island or on the surface of the substrate (diethylene glycol); ii. detaching of a NP from edges of an island; iii. switching positions between two NPs. We assumed that the OA/PS-Fe_3O_4 and MOF NPs locate randomly in a drop at the initial state (Figures 3a and 3b). The diffusion process (related to the interaction energy) kinetically results in different self-assembly behaviors by using the interaction values calculated by DFT (calculation details are in the supporting information). Figure 3c and 3d showed the intermediate state, where the three layers of NPs diffuse toward the interface, indicating the final patterns. The simulations are considered to be at equilibrium when the fractions of nanoparticles in each layer no longer change; the final states are shown in Figures 3e and 3f. The at-equilibrium and self-assembled patterns agree well with the experiment results in Figure 2. In the self-assembly process using OA-Fe_3O_4 NCs and MOF NPs, the MC model showed that the OA-Fe_3O_4 NCs move faster than MOF, thus assembling into the first layer at the bottom, resulting in a separated bilayer structure with MOF sitting on top of the Fe_3O_4 layer. With stronger interaction energy, PS has a relatively sluggish dynamics of chain motions, which hinder the diffusion kinetics of the PS- Fe_3O_4 NCs; the resulting PS- Fe_3O_4 NCs and MOF NPs assemble simultaneously at the same plane. In addition, it is hypothesized that the PS-Fe_3O_4 NCs and MOF form strong bonds between each other, and thus result in a mixture of PS-Fe_3O_4 and MOF in a single layer structure.

Our experimental observations along with theoretical modeling and simulations have together elucidated an understanding of a complicated self-assembly process using a MOF and an inorganic nanocrystal. This study demonstrates that MOFs can be incorporated into self-assembled superstructures. Along with the in-depth understanding of the self-assembly process by simulations, this study introduces a new method for designing multi-functional superstructures controlled by ligand interaction.

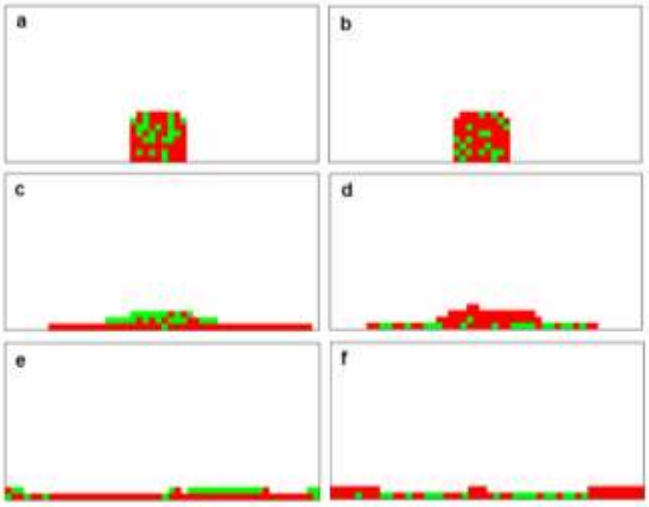

Figure 3. Simulated MC images of OA/PS-Fe_3O_4 and MOF self-assembly processes. a, c, e are initial state for OA-Fe_3O_4 and MOF NPs in a drop; simulated intermediate state and simulated final states in the self-assembly process, respectively. **b, d, f** are initial state for PS-Fe_3O_4 and MOF NPs in a drop; simulated intermediate state and simulated final states in the self-assembly process, respectively. The red blocks represent Fe_3O_4 NCs, while the green blocks represent MOF NPs

References

1. Xia, W.; Mahmood, A.; Zou, R. Q.; Xu, Q., Metal-organic frameworks and their derived nanostructures for electrochemical energy storage and conversion. *Energy & Environmental Science* **2015,** *8* (7), 1837-1866.
2. Li, J.; Wang, Y. C.; Zhou, T.; Zhang, H.; Sun, X. H.; Tang, J.; Zhang, L. J.; Al-Enizi, A. M.; Yang, Z. Q.; Zheng, G. F., Nanoparticle Superlattices as Efficient Bifunctional Electrocatalysts for Water Splitting. *J Am Chem Soc* **2015,** *137* (45), 14305-14312.
3. Chen, L. Y.; Luque, R.; Li, Y. W., Controllable design of tunable nanostructures inside metal-organic frameworks. *Chemical Society Reviews* **2017,** *46* (15), 4614-4630.

4. Choi, J. H.; Fafarman, A. T.; Oh, S. J.; Ko, D. K.; Kim, D. K.; Diroll, B. T.; Muramoto, S.; Gillen, J. G.; Murray, C. B.; Kagan, C. R., Bandlike Transport in Strongly Coupled and Doped Quantum Dot Solids: A Route to High-Performance Thin-Film Electronics. *Nano Lett* **2012,** *12* (5), 2631-2638.
5. Shevchenko, E. V.; Ringler, M.; Schwemer, A.; Talapin, D. V.; Klar, T. A.; Rogach, A. L.; Feldmann, J.; Alivisatos, A. P., Self-assembled binary superlattices of CdSe and Au nanocrystals and their fluorescence properties. *J Am Chem Soc* **2008,** *130* (11), 3274-+.
6. Kang, Y. J.; Ye, X. C.; Chen, J.; Cai, Y.; Diaz, R. E.; Adzic, R. R.; Stach, E. A.; Murray, C. B., Design of Pt-Pd Binary Superlattices Exploiting Shape Effects and Synergistic Effects for Oxygen Reduction Reactions. *J Am Chem Soc* **2013,** *135* (1), 42-45.
7. Chen, O.; Riedemann, L.; Etoc, F.; Herrmann, H.; Coppey, M.; Barch, M.; Farrar, C. T.; Zhao, J.; Bruns, O. T.; Wei, H.; Guo, P.; Cui, J.; Jensen, R.; Chen, Y.; Harris, D. K.; Cordero, J. M.; Wang, Z. W.; Jasanoff, A.; Fukumura, D.; Reimer, R.; Dahan, M.; Jain, R. K.; Bawendi, M. G., Magneto-fluorescent core-shell supernanoparticles. *Nat Commun* **2014,** *5*.
8. Ye, X. C.; Fei, J. Y.; Diroll, B. T.; Paik, T.; Murray, C. B., Expanding the Spectral Tunability of Plasmonic Resonances in Doped Metal-Oxide Nanocrystals through Cooperative Cation-Anion Codoping. *J Am Chem Soc* **2014,** *136* (33), 11680-11686.
9. Ye, X. C.; Chen, J.; Diroll, B. T.; Murray, C. B., Tunable Plasmonic Coupling in Self-Assembled Binary Nanocrystal Super lattices Studied by Correlated Optical Microspectrophotometry and Electron Microscopy. *Nano Lett* **2013,** *13* (3), 1291-1297.
10. Urban, J. J.; Talapin, D. V.; Shevchenko, E. V.; Kagan, C. R.; Murray, C. B., Synergismin binary nanocrystal superlattices leads to enhanced p-type conductivity in self-assembled PbTe/Ag-2 Te thin films. *Nature Materials* **2007,** *6* (2), 115-121.
11. Urban, J. J.; Talapin, D. V.; Shevchenko, E. V.; Murray, C. B., Self-assembly of PbTe quantum dots into nanocrystal superlattices and glassy films. *J Am Chem Soc* **2006,** *128* (10), 3248-3255.
12. Shevchenko, E. V.; Talapin, D. V.; Kotov, N. A.; O'Brien, S.; Murray, C. B., Structural diversity in binary nanoparticle superlattices. *Nature* **2006,** *439* (7072), 55-59.
13. Tan, R.; Zhu, H.; Cao, C.; Chen, O., Multi-component superstructures self-assembled from nanocrystal building blocks. *Nanoscale* **2016,** *8* (19), 9944-9961.
14. Shevchenko, E. V.; Talapin, D. V.; Murray, C. B.; O'Brien, S., Structural characterization of self-assembled multifunctional binary nanoparticle superlattices. *J Am Chem Soc* **2006,** *128* (11), 3620-3637.
15. Evers, W. H.; De Nijs, B.; Filion, L.; Castillo, S.; Dijkstra, M.; Vanmaekelbergh, D., Entropy-Driven Formation of Binary Semiconductor-Nanocrystal Superlattices. *Nano Lett* **2010,** *10* (10), 4235-4241.
16. Eldridge, M. D.; Madden, P. A.; Frenkel, D., Entropy-Driven Formation of a Superlattice in a Hard-Sphere Binary Mixture. *Nature* **1993,** *365* (6441), 35-37.
17. Wei, J. J.; Schaeffer, N.; Pileni, M. P., Ligand Exchange Governs the Crystal Structures in Binary Nanocrystal Superlattices. *J Am Chem Soc* **2015,** *137* (46), 14773-14784.
18. Goodfellow, B. W.; Yu, Y. X.; Bosoy, C. A.; Smilgies, D. M.; Korgel, B. A., The Role of Ligand Packing Frustration in Body-Centered Cubic (bcc) Superlattices of Colloidal Nanocrystals. *J Phys Chem Lett* **2015,** *6* (13), 2406-2412.
19. Na, K.; Choi, K. M.; Yaghi, O. M.; Somorjai, G. A., Metal nanocrystals embedded in single nanocrystals of MOFs give unusual selectivity as heterogeneous catalysts. *Nano Lett* **2014,** *14* (10), 5979-83.
20. Furukawa, H.; Gandara, F.; Zhang, Y. B.; Jiang, J.; Queen, W. L.; Hudson, M. R.; Yaghi, O. M., Water adsorption in porous metal-organic frameworks and related materials. *J Am Chem Soc* **2014,** *136* (11), 4369-81.
21. Fracaroli, A. M.; Furukawa, H.; Suzuki, M.; Dodd, M.; Okajima, S.; Gandara, F.; Reimer, J. A.; Yaghi, O. M., Metal-organic frameworks with precisely designed interior for carbon dioxide capture in the presence of water. *J Am Chem Soc* **2014,** *136* (25), 8863-6.

22. Kaye, S. S.; Dailly, A.; Yaghi, O. M.; Long, J. R., Impact of preparation and handling on the hydrogen storage properties of Zn4O(1,4-benzenedicarboxylate)(3) (MOF-5). *J Am Chem Soc* **2007,** *129* (46), 14176-+.
23. Dong, A. G.; Chen, J.; Vora, P. M.; Kikkawa, J. M.; Murray, C. B., Binary nanocrystal superlattice membranes self-assembled at the liquid-air interface. *Nature* **2010,** *466* (7305), 474-477.

Supplementary Information is available in the online version of the paper.

Acknowledgements: This work was supported by the Molecular Foundry and the Advanced Light Source at Lawrence Berkeley National Laboratory, both user facilities supported by the Office of Science, Office of Basic Energy Sciences, of the U.S. Department of Energy (DOE) under Contract No. DE-AC02-05CH11231. F.Q. and J. J. Urban acknowledge….Y. F. Z. and S. D. acknowledge National Nature Science Foundation of China (No. 51325204).

Author Contributions: F. Q. and J. J. Urban designed, led the project and wrote the paper. F. Q. performed the experimental works including synthesis, self-assembly, characterizations. Y. F. Z., and G. L. performed the simulation work. A. P. synthesized polystyrene-COOH. C. H. C. and S. J. contributed to design of cartoons in the figures. T. M. M. performed X-ray Diffraction. M. B. performed Resonant soft x-ray scattering. C. S. contributed to the electron tomography. P. E. performed the tomography reconstruction. K. B. contributed to STEM/EDX. S. W., J. N., and S. D. served as PI and primary advisor for the simulation. All authors discussed the results and contributed to the manuscript.

Author Information:

 Correspondence and requests for materials should be addressed to J. J. U. (email: jjurban@lbl.gov)